

Influence of cold deformation and Ti element on the microstructure and properties of Cu–Cr system alloys

Pengchao Zhang, Jinchuan Jie,^{a)} Yuan Gao, Hang Li, Tongmin Wang,^{b)} and Tingju Li
School of Materials Science and Engineering, Laboratory of Special Processing of Raw Materials, Dalian University of Technology, Dalian 116024, China

(Received 12 January 2015; accepted 28 April 2015)

The Cu–Cr system alloys with different Ti contents were prepared and processed by deformation and heat treatment. The microstructures, mechanical, and electrical properties were investigated under as-cast and aged conditions. The results indicate that the Cr precipitates present a dispersed distribution and exhibit a face-centered cubic (fcc) structure rather than equilibrium body-centered cubic (bcc) structure in the initial stage of aging. A certain amount of Ti atoms dissolves in matrix due to the large solid solubility, while the remaining atoms segregate around the interface of the Cr precipitates to form a sandwich structure. Improvement of mechanical properties is achieved with Ti addition and the increasing rolling reduction, which can be ascribed to multiple mechanisms. In addition, Ti has a negative effect on the electrical conductivity, while deformation has a slight effect on conductivity.

I. INTRODUCTION

Copper alloys with excellent mechanical properties and electrical conductivity have received a great deal of attention and obtained wide applications in recent years.^{1–8} In particular, Cu–Cr alloy is one of the most important commercial metallic materials due to their favorable electrical properties under appropriate heat treatment.⁹ But the mechanical performance is limited because of the low solubility of Cr in the matrix.¹⁰ The tensile strength of Cu–Cr alloy is less than 500 MPa, which cannot meet the qualification of integrated circuit lead frame and electrical contact.^{11,12}

Alloying is a common approach to improve the mechanical performance of Cu–Cr alloy. Various minor elements, such as Zr, Mg, Ag, and Ti, have been added to Cu–Cr alloy to achieve this objective.^{1,11,13,14} Ti is an available alloying element in view of low melting loss and cost. Nagesha et al. investigated the properties of Cu–Cr–Zr–Ti alloy under low-cycle fatigue deformation.¹⁴ Wang et al. reported that Ti element can refine Cr particles during annealing process.¹⁵ In addition, most of the high strength copper alloys have to undergo the deformation process to further increase mechanical properties, and cold rolling has a good effect on strengthening as an effective deformation method.^{16,17} Besides, the varying degrees of deformation can produce different results of strengthening effect.¹⁸ However, alloying and

deformation can result in the decline of conductivity, while it improves the mechanical properties.^{11,17} The electrical conductivity is necessary to be considered in industrial applications since an acceptable conductivity can reduce the loss of electric energy. So a compromised performance of mechanical and electrical properties should be adopted to acquire the comprehensive performance.

In the present study, the microstructure and properties of Cu–Cr–Ti alloys after cold rolling and aging treatment were studied. Attempts were made to investigate the effect of Ti content and degree of deformation on the microstructure and properties of Cu–Cr system alloys.

II. EXPERIMENTAL PROCEDURE

Four Cu–Cr system alloys were prepared with electrolytic copper (99.97 wt%), pure chromium (99.8 wt%), and pure titanium (99.5 wt%) in an intermediate frequency induction furnace. The compositions are listed in Table I.

The ingots were homogenized at 850 °C and rapidly hot rolled to a thickness of 10 mm. Then, the plates were solution treated at 920 °C for 30 min, followed by water quenching. The specimens were planed on both sides to remove surface defects, and then cut into small samples. The samples were cold rolled with 60, 70, 80, and 90% reductions and subsequently isothermally aged at 450 °C for various times. Processes A, B, C, and D corresponding to the deformation reductions of 60, 70, 80, and 90% were labeled, respectively.

The specimens were polished and etched in a FeCl₃ solution. The microstructures were characterized by

Contributing Editor: Jürgen Eckert

Address all correspondence to these authors.

^{a)}e-mail: jiejc@dlut.edu.cn

^{b)}e-mail: tmwang@dlut.edu.cn

DOI: 10.1557/jmr.2015.143

TABLE I. Chemical composition of the prepared Cu–Cr–Ti alloys (wt%).

Alloy	Cr	Ti	Cu
Cu–0.5Cr	0.52	...	Bal.
Cu–0.5Cr–0.05Ti	0.52	0.06	Bal.
Cu–0.5Cr–0.1Ti	0.48	0.1	Bal.
Cu–0.5Cr–0.18Ti	0.51	0.18	Bal.

optical microscope (OM, MEF4, Leica company, Solms, Germany) and field emission scanning electron microscope (FESEM, SUPRA55, Carl Zeiss company, Oberkochen, Germany) equipped with an energy dispersion spectrometer (EDS). For transmission electron microscopy (TEM) observation, thin foils were ground to 30 μm in thickness and subjected to low-angle ion milling with an argon ion beam. The microstructures of TEM examination and selected area electron diffraction (SAED) were carried out by TEM (JEM-2100F, JEOL company, Tokyo, Japan).

Tensile tests were conducted on a computerized universal testing machine, and the fracture morphology was also observed by FESEM. Vickers hardness was tested on a MH-5L type microhardness tester with a load of 200 g and loading time of 15 s. Electrical conductivity was measured by a D60K conductivity measuring instrument, and it was characterized by International Annealed Copper Standard (%IACS). The resistivity is obtained by taking the reciprocal of conductivity.

III. RESULTS

A. Microstructure

The optical micrographs of Cu–0.5Cr–0.18Ti alloy under different conditions are shown in Fig. 1. The microstructure is composed of coarse columnar crystals at an as-cast state [Fig. 1(a)]. After cold rolling, the columnar crystals bend toward the rolling direction at higher rolling reduction and gradually evolve into strip-like morphology [Figs. 1(b) and 1(d)]. When the reduction is up to 90%, the morphology of alloy is fibrous stripes due to the large deformation [Fig. 1(d)]. In a transverse section, the grains become flattened because of the high rolling force [Fig. 1(c)].

Figure 2 shows the TEM image and SAED pattern of Cu–0.5Cr–0.18Ti alloy after aging at 450 $^{\circ}\text{C}$ for 60 min. Plenty of precipitates exhibit dispersive distribution in matrix [Fig. 2(a)]. The corresponding SAED pattern of the alloy is shown in Fig. 2(b). Additional diffraction spots (marked with arrow) are observed in the pattern. It is found that the structure of precipitates is almost the same as that of the matrix, namely the fcc structure. The lattice parameter of the precipitates corresponding to these diffraction spots is calculated to be 0.4143 nm. In previous studies, Huh et al.¹⁹ theoretically predicted that the cell constant of the fcc Cr cluster is 0.413 nm, and Xia et al.¹⁷ deduced from the diffraction spots that the lattice

parameter is 0.4219 nm, which is in accordance with the result of this work. So the dispersed particles in matrix are fcc Cr precipitates, which are derived from matrix during aging treatment as the solubility of Cr in the Cu matrix decreases with the decreasing temperature. Besides, the precipitates have a crystal cell larger than that of the matrix, revealing a cube-on-cube orientation relationship with the matrix.¹⁷

The SEM images of Cu–0.5Cr–0.18Ti alloy after different rolling reductions and aging at 450 $^{\circ}\text{C}$ for 120 min are shown in Fig. 3. The grain size along the direction of rolling force dramatically reduces, and the strip texture is further refined with increasing deformation. The Cr precipitates are dispersed in the matrix after aging with two kinds of reductions, and some precipitates become coarsened (points A and C) after aging for 120 min. As the EDS analysis shown in Table II, a number of Ti atoms presents segregation in the interface between Cr particles and matrix to form a sandwich structure (points A and C), and the remaining atoms dissolve in matrix to form a solid solution (points B and D).

B. Mechanical and electrical properties

The hardness curve of 90% cold-rolled Cu–Cr system alloys isothermally aged at 450 $^{\circ}\text{C}$ is exhibited in Fig. 4(a). The hardness of Cu–Cr alloy reaches the peak after aging for 120 min and then decreases with increasing aging time, while that of Cu–Cr–Ti alloys increases quickly at the initial stage and then maintains at a high plateau. The presence of Ti even in small amount dramatically improves the hardness of alloy. With increasing Ti content from 0.1 to 0.18 wt%, no significant increment in hardness is observed. Figure 4(b) presents the hardness of Cu–0.5Cr–0.18Ti alloy after different rolling reductions and isothermal aging at 450 $^{\circ}\text{C}$. From an overall perspective, the hardness improves with an increase in the rolling reduction. The variations of hardness versus aging time under every rolling reduction are exactly similar, exhibiting an initial increase followed by a mild ascent after aging for 150 min.

The yield strength, ultimate tensile strength (UTS), and elongation of aged Cu–Cr system alloys with different Ti contents and various cold deformations are shown in Fig. 5. The Cu–Cr alloy after aging possesses the UTS of 493 MPa and good ductility. It is evident that Cu–Cr–Ti alloys have superior strength compared with Cu–Cr alloy, and the tensile strength is enhanced with the increasing Ti content. However, the increment of UTS is minor as the Ti content exceeds 0.1 wt%. The elongation presents a significant reduction with the addition of Ti as a response of the improved strength. The increment of tensile strength about Cu–0.5Cr–0.18Ti along diverse rolling reductions is noticeable. High strength is found to benefit from more serious deformation. But the elongation reduces with the increase of deformation in response to the excellent strength.

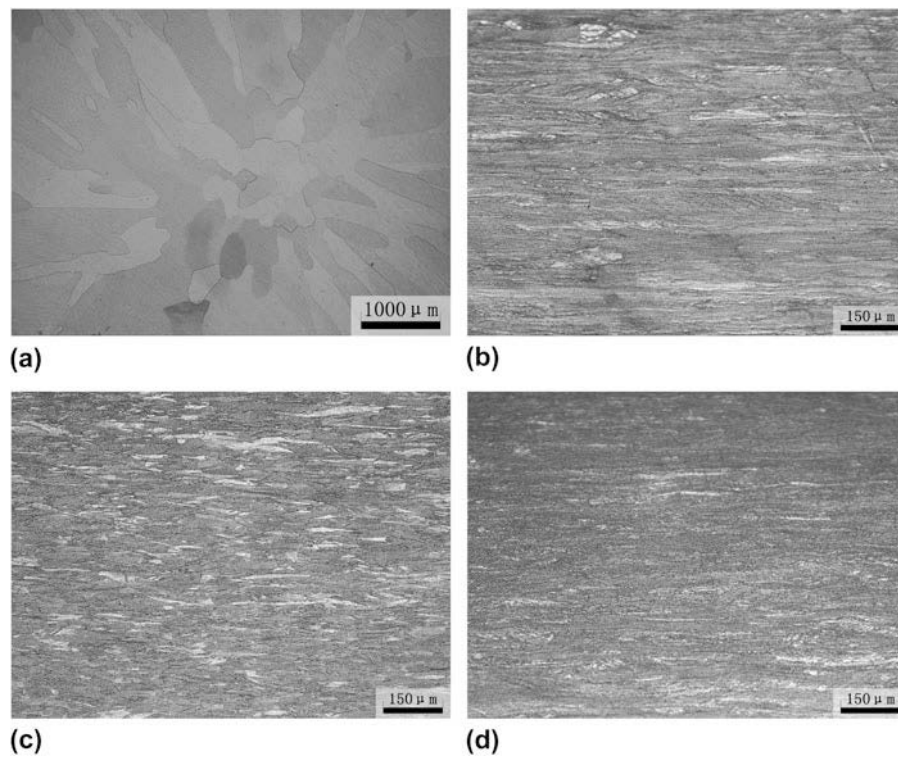


FIG. 1. Optical micrographs of Cu–0.5Cr–0.18Ti alloy under as-cast conditions and aging at 450 °C for 60 min with different rolling reductions: (a) As-cast, (b) process C, longitudinal section, (c) process C, transverse section, and (d) process D, longitudinal section.

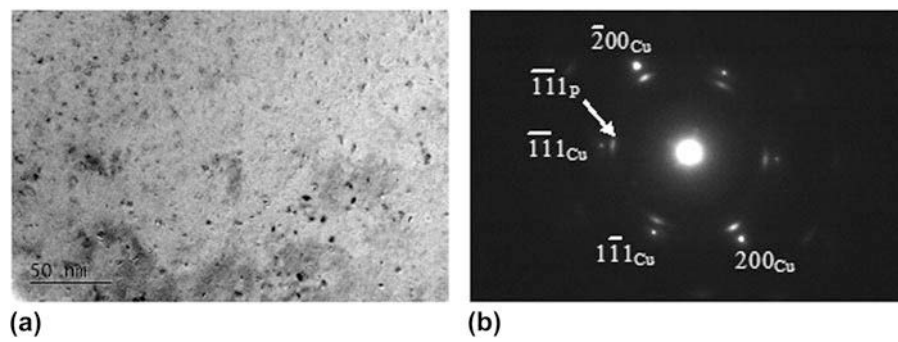


FIG. 2. TEM micrograph and SAED pattern of Cu–0.5Cr–0.18Ti alloy aged at 450 °C for 60 min: (a) Bright field image and (b) SAED pattern with zone axis [011]_{Cu}.

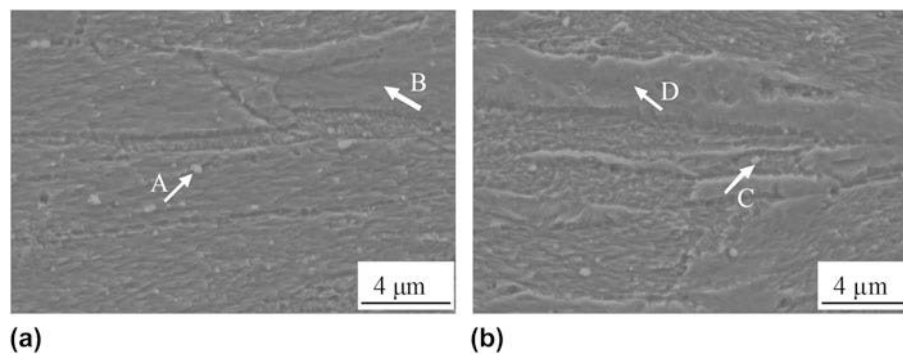


FIG. 3. SEM images of Cu–0.5Cr–0.18Ti alloy after different rolling reductions and aging at 450 °C for 120 min: (a) Process C, transverse section and (b) process D, transverse section.

TABLE II. The EDS results of Cu–Cr–Ti alloys at different points as shown in Fig. 3.

Spectrum point	Cu (wt%)	Cr (wt%)	Ti (wt%)
A	71.13	28.52	0.35
B	99.85	...	0.15
C	74.19	25.37	0.44
D	99.86	...	0.14

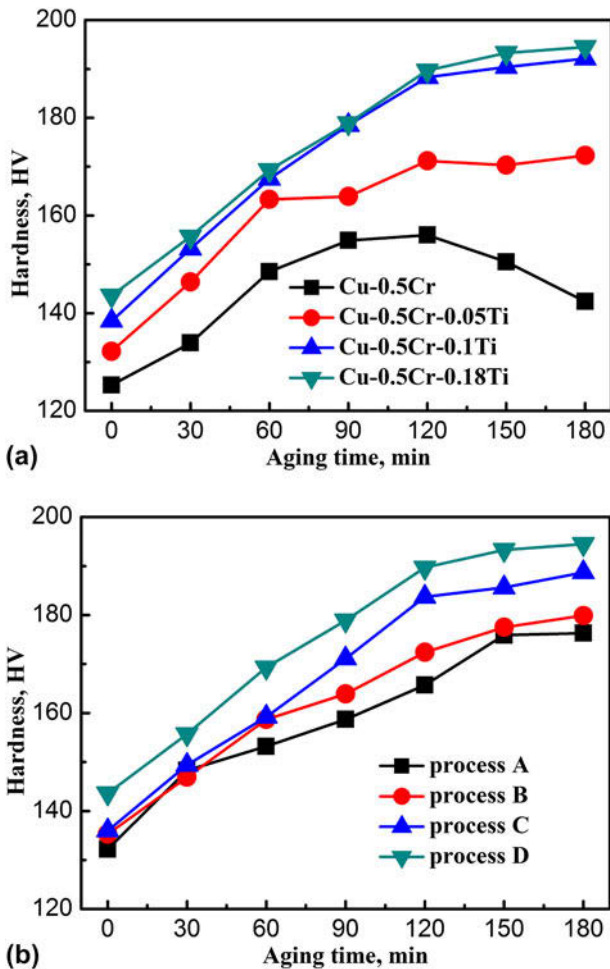


FIG. 4. Hardness of Cu–Cr–Ti alloys under different conditions: (a) Cu–Cr system alloys isothermally aged at 450 °C, process D and (b) Cu–0.5Cr–0.18Ti alloy after different rolling reductions and isothermal aging at 450 °C.

The tensile fracture surfaces of Cu–Cr system alloys with various rolling reductions are presented in Fig. 6. The presence of dimples can be identified from the fracture surface of Cu–0.5Cr alloy with 80% rolling reduction [Fig. 6(a)]. Such type of fractography is typical ductile fracture, which is generated by the formation, growth, and coalescence of microvoids during the necking process in the course of tensile deformation. Shallow dimples are observed in the fractography of Cu–0.5Cr alloy with 90% reduction [Fig. 6(b)],

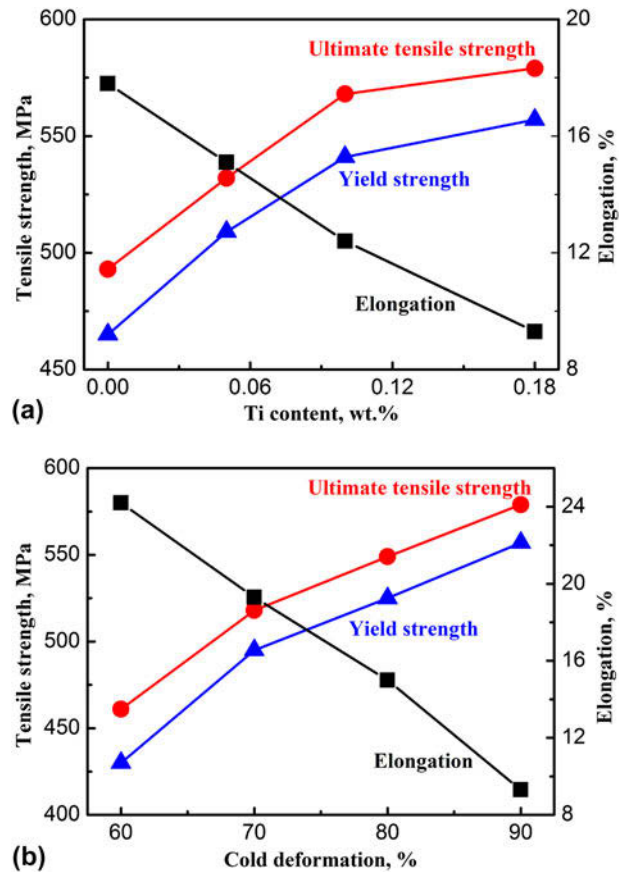


FIG. 5. Tensile properties of Cu–Cr–Ti alloys under different conditions: (a) Cu–Cr system alloys aged at 450 °C for 120 min, process D and (b) Cu–0.5Cr–0.18Ti alloy after different rolling reductions, and aging at 450 °C for 120 min.

indicating a reduced toughness under severe plastic deformation. The fracture surface of Cu–0.5Cr–0.18Ti alloy shows lower dimples [Fig. 6(c)] compared with Cu–Cr alloy, suggesting a decreased elongation with the addition of Ti element. After large deformation of the above alloy, a series of tiny dimples aggregate to form the dominant feature of fracture morphology [Fig. 6(d)], and the elongation is deteriorated.

The electrical conductivity curves of Cu–Cr system alloys after 90% rolling reduction and aging at 450 °C for various times are shown in Fig. 7(a). The Cu–Cr alloy possesses excellent conductivity, which is 8.8 %IACS and 22.1 %IACS greater than that of the alloys with 0.05 wt% Ti and 0.1 wt% Ti, respectively, after aging for 180 min. For Cu–0.5Cr and Cu–0.5Cr–0.05Ti alloys, a fast raise in conductivity during the initial stage of aging can be seen owing to the decomposition of the supersaturated solid solution. The increment in conductivity is slow after aging for 60 min, and the conductivity nearly remains stable after 150 min. The conductivity of alloys with 0.1 and 0.18 wt% Ti presents a gradual enhancement during aging. Figure 7(b) exhibits the

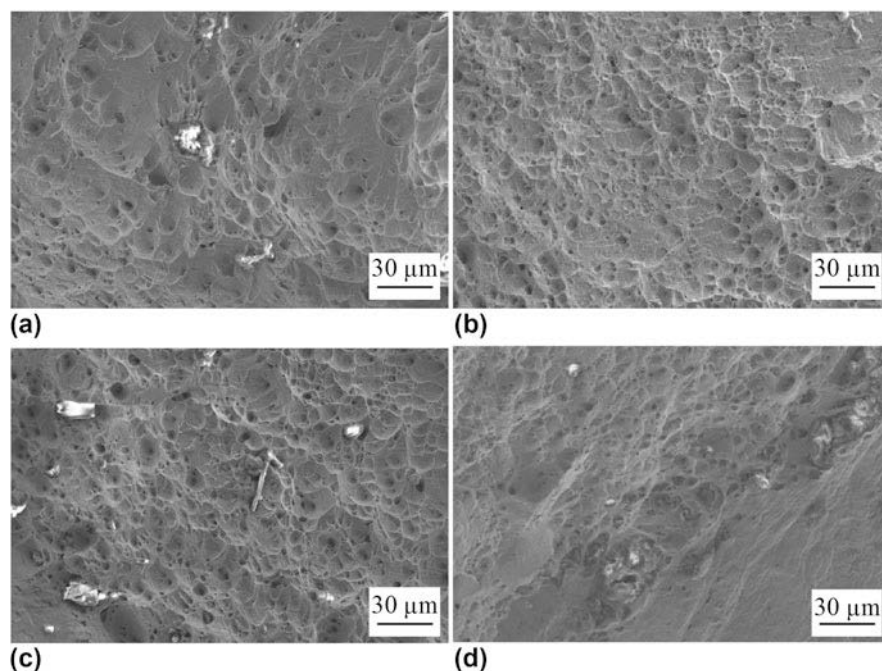


FIG. 6. SEM micrographs of the fracture surfaces of Cu–Cr system alloys aged at 450 °C for 120 min: (a) Cu–0.5Cr, process C, (b) Cu–0.5Cr, process D, (c) Cu–0.5Cr–0.18Ti, process C, and (d) Cu–0.5Cr–0.18Ti, process D.

conductivity curves of Cu–0.5Cr–0.18Ti with different rolling reductions. A marginally downward trend of conductivity is obtained with the increasing deformation. The conductivity of Cu–0.5Cr–0.18Ti reaches 54.9 % IACS after 90% rolling reduction and aging at 450 °C for 180 min, which is just 0.2 %IACS and 1.7 %IACS lower than that of the alloys with 80 and 60% deformation, respectively.

IV. DISCUSSION

A. The formation of microstructure of Cu–Cr system alloys

The microstructure of Cu–Cr system alloys significantly changes after plastic deformation. The coarse crystals elongate along the rolling direction. The grains are replaced by fibrous textures and possess an increased aspect ratio with severe plastic deformation.

For Cu–Cr system alloys, due to the limited solubility of Cr atoms in Cu matrix, Cr particles are precipitated and dispersed in matrix after aging. The Cr precipitates exhibit the fcc structure rather than the equilibrium bcc in the initial stage of aging. This is because the structure of nanoscale Cr precipitate is determined by cluster energy.¹⁹ The surface energy is a critical factor in determining the cluster energy due to the great surface-to-volume ratio of nanoscale cluster. Fewer surface atoms are needed for fcc structure, which is ascribed to the higher packing fraction of fcc structure (0.74) than the bcc structure (0.68). However, the surface-to-volume

ratio is reduced with the coarsening of Cr precipitate and even becomes negligible with the extended aging time. Then the precipitate transforms into its inherent bcc structure.¹⁹

Due to the large solubility of Ti in Cu matrix, a certain amount of Ti atoms dissolve in matrix. The remaining Ti atoms segregate around the interface of Cr precipitates to form a sandwich structure. The reason for this phenomenon is that the phase boundaries between the coarse Cr precipitates and matrix get incoherent with increasing aging time. In response, a large amount of vacancies and/or dislocations are generated in the interface regions²⁰ and easy diffusion paths for dissolved Ti atoms are formed.²¹ Following this, the sandwich structure is developed owing to the segregation of Ti atoms in the interface of Cr particles.

B. Effects of Ti element and plastic deformation on mechanical properties of Cu–Cr system alloys

Cold rolling brings high density dislocations, which can significantly improve hardness of Cu–Cr system alloys. Dislocations interact with each other and tangle together to impede their own motion.²² Hence, high density dislocations are capable of improving the mechanical properties of metal. Besides strain hardening, grain refinement strengthening mechanism also plays a role in improving mechanical properties during rolling process. Cold rolling refines the grains and generates a high density of grain boundaries, which can increase the hardness and tensile strength.^{23,24}

In brief, the increased mechanical properties after cold rolling can be attributed to the interaction of strain hardening and grain refinement strengthening.

After aging, the supersaturated Cu–Cr system alloys decompose, and the Cr particles are precipitated from the metastable alloys. The precipitates have a great effect on pinning subgrain boundaries and dislocations, which can impede the migration of boundaries and accelerate the accumulation of dislocations inside the grains. Then, the hardness is further improved owing to the precipitation hardening. Meanwhile, the strength is also reinforced by the contribution of precipitation strengthening. Ellis and Michal reported that Orowan stress is inversely proportional to the interprecipitate spacing in the strengthening mechanism.²⁵ The coarsening of precipitates can result in the increase of interprecipitate space. So the hardness of Cu–Cr system alloy merely exhibits slight rising and even declines with the increasing aging time.

It is noticeable that since Ti element added to Cu–Cr alloy, the mechanical properties are evidently enhanced in various states, which can be attributed to solid solution strengthening mechanism. A certain amount of Ti atoms

dissolves in Cu matrix, and the motion of dislocations is impeded owing to the variation of strain fields,²⁶ thereby improving the mechanical properties.

In conclusion, the excellent mechanical properties can be attributed to multiple mechanisms. Figure 8 summarizes the hardening mechanisms of Cu–Cr system alloys under different conditions. The significant hardness of Cu–Cr–Ti alloy is ascribed to multiple mechanisms, comprising of precipitation hardening of Cr precipitates, solid solution strengthening of dissolved Ti atoms in matrix, strain hardening, and grain refinement strengthening from deformation process. Similar to hardness, the tensile strength also benefits from above mechanisms.

C. Effects of Ti element and plastic deformation on conductivity of Cu–Cr system alloys

The conductivity of whole Cu–Cr system alloys presents an upward trend during the initial period of aging and maintains a relatively steady state after aging for 150 min. Due to the inverse relationship between conductivity and resistivity, the conductivity can be characterized by the contribution of four scattering mechanisms of resistivity:²⁷

$$1/\sigma_{\text{alloy}} = \rho_{\text{alloy}} = \rho_{\text{pho}} + \rho_{\text{def}} + \rho_{\text{int}} + \rho_{\text{imp}} \quad (1)$$

where σ_{alloy} and ρ_{alloy} are the conductivity and resistivity of Cu–Cr system alloys, and ρ_{pho} , ρ_{def} , ρ_{int} , and ρ_{imp} are the resistivity contributions from phonon scattering, defect scattering, interface scattering, and impurity scattering, respectively.

Temperature is the only influential factor of phonon scattering. The phonon scattering is equal because the resistivity of all specimens is measured at the same temperature. Experiments of alloys with different compositions have shown that the conductivity presents progressive decrease with the increasing Ti content, implying that the dissolved Ti atoms have a large impact

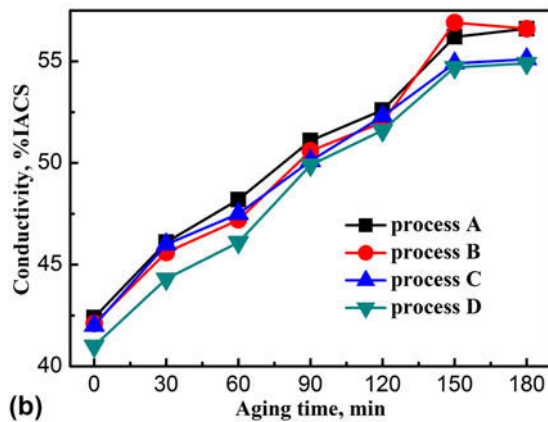
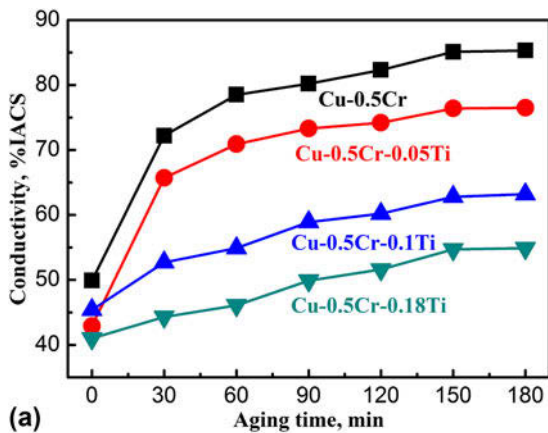


FIG. 7. Conductivity of Cu–Cr–Ti alloys under different conditions: (a) Cu–Cr system alloys isothermally aged at 450 °C, process D, (b) Cu–0.5Cr–0.18Ti alloy after different rolling reductions and isothermal aging at 450 °C.

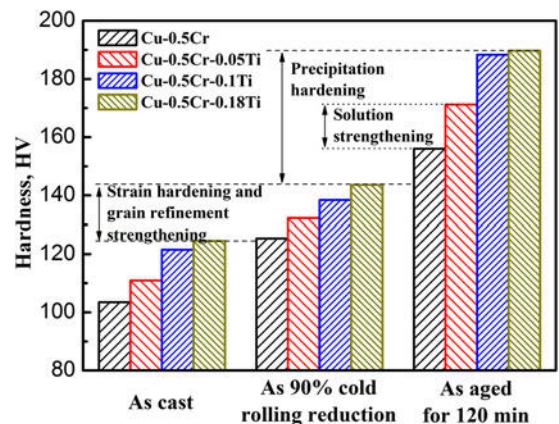


FIG. 8. The multiple hardening mechanisms of Cu–Cr system alloys under different conditions.

on the impurity scattering. During the initial aging process, the conductivity presents an increasing trend, which is attributed to gradually reduced impurity scattering accompanied by the precipitation of Cr particles. With aging time increasing to 150 min, the conductivity is basically stable owing to the absence of dissolved Cr atoms in matrix. The impurity scattering from dissolved Cr atoms progressively weakens, while the interface scattering from precipitated Cr particles intensifies throughout the aging process. But overall, the conductivity increases under the combined action of the two mechanisms, signifying that the solute atoms possess intense scattering effect for conduction electron, while the contribution from interface scattering is less prominent.

For the Cu–0.5Cr–0.18Ti alloy, mechanical deformation can introduce fine grains and plentiful defects, intensifying the extent of scattering electrical resistivity. However, only a modest decline is observed with deformation. The phenomenon shows that the effects of interface and defect scattering are not remarkable on resistivity.

In brief, the resistivity of Cu–Cr–Ti alloy is affected by the action of multiple scattering mechanisms. The impurity scattering from dissolved Ti atoms plays a leading role, while the interface and defect scattering have a moderate influence on electrical behavior.

V. CONCLUSIONS

(1) Cr precipitates present a dispersed distribution and exhibit the fcc structure rather than equilibrium bcc structure in the initial stage of aging. A certain amount of Ti atoms dissolve in matrix, while the remaining atoms segregate around the interface of Cr precipitates to form a sandwich structure.

(2) The mechanical properties of Cu–Cr–Ti alloys are positively correlated with the increasing Ti content and deformation degree, which can be ascribed to multiple mechanisms. The excellent hardness of Cu–Cr–Ti alloy is obtained due to the comprehensive mechanisms, comprising of precipitation hardening of Cr precipitates, solid solution strengthening of dissolved Ti atoms in the matrix, strain hardening, and grain refinement strengthening from deformation process.

(3) The added Ti element reduces the conductivity of Cu–Cr system alloys, while the deformation has a slight effect on conductivity. This indicates that the impurity scattering from dissolved Ti atoms plays a leading role while the interface and defect scattering have a moderate influence on electrical behavior.

ACKNOWLEDGMENTS

The authors gratefully acknowledge the support of the Natural Science Foundation of China (Nos. 51134013, 51271042) and the Fundamental Research Funds for the Central Universities of China (DUT14RC(4)13).

REFERENCES

1. D. Raabe, K. Miyake, and H. Takahara: Processing, microstructure, and properties of ternary high-strength Cu–Cr–Ag in situ composites. *Mater. Sci. Eng., A* **291**, 186 (2000).
2. K. Maki, Y. Ito, H. Matsunaga, and H. Mori: Solid-solution copper alloys with high strength and high electrical conductivity. *Scr. Mater.* **68**, 777 (2013).
3. N. Takata, S.H. Lee, and N. Tsuji: Ultrafine grained copper alloy sheets having both high strength and high electric conductivity. *Mater. Lett.* **63**, 1757 (2009).
4. J.H. Su, P. Liu, Q.M. Dong, H.J. Li, and F.Z. Ren: Aging study of rapidly solidified and solid-solution Cu–Cr–Sn–Zn alloy. *J. Mater. Process. Technol.* **205**, 366 (2008).
5. J.Q. Deng, X.Q. Zhang, S.Z. Shang, F. Liu, Z.X. Zhao, and Y.F. Ye: Effect of Zr addition on the microstructure and properties of Cu–10Cr in situ composites. *Mater. Des.* **30**, 4444 (2009).
6. C.D. Xia, Y.L. Jia, W. Zhang, K. Zhang, Q.Y. Dong, G.Y. Xu, and M.P. Wang: Study of deformation and aging behaviors of a hot rolled–quenched Cu–Cr–Zr–Mg–Si alloy during thermomechanical treatments. *Mater. Des.* **39**, 404 (2012).
7. L.P. Deng, K. Han, K.T. Hartwig, T.M. Siegrist, L.Y. Dong, Z.Y. Sun, X.F. Yang, and Q. Liu: Hardness, electrical resistivity, and modeling of in situ Cu–Nb microcomposites. *J. Alloys Compd.* **602**, 331 (2014).
8. Q. Lei, Z. Li, J. Wang, J.M. Xie, X. Chen, S. Li, Y. Gao, and L. Li: Hot working behavior of a super high strength Cu–Ni–Si alloy. *Mater. Des.* **51**, 1104 (2013).
9. J.H. Su, P. Liu, H. Li, F.Z. Ren, and Q.M. Dong: Phase transformation in Cu–Cr–Zr–Mg alloy. *Mater. Lett.* **61**, 4963 (2007).
10. Z.P. Que, J.H. Lee, H.M. Jung, J.H. Shin, S.Z. Han, and K.J. Euh: Microstructure evolution in Cu–1.54wt% Cr alloy during directional solidification. *J. Cryst. Growth* **362**, 58 (2013).
11. Y. Pang, C.D. Xia, M.P. Wang, Z. Li, Z. Xiao, H.G. Wei, X.F. Sheng, Y.L. Jia, and C. Chen: Effects of Zr and (Ni, Si) additions on properties and microstructure of Cu–Cr alloy. *J. Alloys Compd.* **582**, 786 (2014).
12. C. Watanabe, R. Monzen, and K. Tazaki: Mechanical properties of Cu–Cr system alloys with and without Zr and Ag. *J. Mater. Sci.* **43**, 813 (2008).
13. J.H. Su, Q.M. Dong, P. Liu, H.J. Li, and B.X. Kang: Research on aging precipitation in a Cu–Cr–Zr–Mg alloy. *Mater. Sci. Eng., A* **392**, 422 (2005).
14. A. Nagesha, P. Parameswaran, A. Biswas, R. Sandhya, A.K. Asraff, and M.D. Mathew: Microstructural investigations into the low cycle fatigue deformation of a Cu–Cr–Zr–Ti alloy. *Mater. Sci. Eng., A* **582**, 91 (2013).
15. Y.H. Wang, X.P. Song, Z.B. Sun, X. Zhou, and J. Guo: Effects of Ti addition on microstructures of melt-spun CuCr ribbons. *Trans. Nonferrous Met. Soc. China* **17**, 72 (2007).
16. K.X. Wei, W. Wei, F. Wang, Q.B. Du, I.V. Alexandrov, and J. Hu: Microstructure, mechanical properties and electrical conductivity of industrial Cu–0.5%Cr alloy processed by severe plastic deformation. *Mater. Sci. Eng., A* **528**, 1478 (2011).
17. C.D. Xia, W. Zhang, Z.Y. Kang, Y.L. Jia, Y.F. Wu, R. Zhang, G.Y. Xu, and M.P. Wang: High strength and high electrical conductivity Cu–Cr system alloys manufactured by hot rolling–quenching process and thermomechanical treatments. *Mater. Sci. Eng., A* **538**, 295 (2012).
18. N.K. Tewary, S.K. Ghosh, S. Bera, D. Chakrabarti, and S. Chatterjee: Influence of cold rolling on microstructure, texture and mechanical properties of low carbon high Mn TWIP steel. *Mater. Sci. Eng., A* **615**, 405 (2014).
19. S.H. Huh, H.K. Kim, J.W. Park, and G.H. Lee: Critical cluster size of metallic Cr and Mo nanoclusters. *Phys. Rev. B* **62**, 2937 (2000).

20. M. Hatakeyama, T. Toyama, J. Yang, Y. Nagai, M. Hasegawa, T. Ohkubo, M. Eldrup, and B.N. Singh: 3D-AP and positron annihilation study of precipitation behavior in Cu–Cr–Zr alloy. *J. Nucl. Mater.* **386–388**, 852 (2009).
21. J.J. Hoyt: On the coarsening of precipitates located on grain boundaries and dislocations. *Acta Metall. Mater.* **39**, 2091 (1991).
22. J.E. Bailey and P.B. Hirsch: The dislocation distribution, flow stress, and stored energy in cold worked polycrystalline silver. *Philos. Mag.* **5**, 485 (1960).
23. L. Gao, R.S. Chen, and E.H. Han: Effects of rare-earth elements Gd and Y on the solid solution strengthening of Mg alloys. *J. Alloys Compd.* **481**, 379 (2009).
24. B. Sun, S. Li, H. Imai, T. Mimoto, J. Umeda, and K. Kondoh: Fabrication of high-strength Ti materials by in-process solid solution strengthening of oxygen via P/M methods. *Mater. Sci. Eng., A* **563**, 95 (2013).
25. D.L. Ellis and G.M. Michal: Precipitation strengthened high strength, high conductivity Cu–Cr–Nb alloys produced by chill block melt spinning. NASA Contractor Reports Server. 185144, (1989).
26. R.L. Fleischer: Solution hardening by tetragonal distortions: Application to irradiation hardening in F.C.C. crystals. *Acta Metall.* **10**, 835 (1962).
27. L. Qu, E.G. Wang, K. Han, X.W. Zuo, L. Zhang, P. Jia, and J.C. He: Studies of electrical resistivity of an annealed Cu–Fe composite. *J. Appl. Phys.* **113**, 173708 (2013).